

**Influences of pH and metal ions on the interactions of  
oxytetracycline onto nano-hydroxyapatite and their  
co-adsorption behavior in aqueous solution**

Lei Yuan <sup>a,1</sup>, Ming Yan <sup>a,1</sup>, Zhenzhen Huang <sup>a,1</sup>, Kai He <sup>a,1</sup>, Guangming Zeng <sup>a,\*</sup>,  
Anwei Chen <sup>b,\*</sup>, Liang Hu <sup>c</sup>, Hui Li <sup>a</sup>, Min Peng <sup>a</sup>, Tiantian Huang <sup>a</sup>, Guiqiu Chen <sup>a</sup>

<sup>a</sup> College of Environmental Science and Engineering, Hunan University and Key  
Laboratory of Environmental Biology and Pollution Control (Hunan University),  
Ministry of Education, Changsha 410082, PR China

<sup>b</sup> College of Resources and Environment, Hunan Agricultural University, Changsha  
410128, PR China

<sup>c</sup> School of Minerals Processing and Bioengineering, Key Laboratory of  
Biohydrometallurgy of Ministry of Education, Central South University, Changsha  
410083, China

\* Corresponding author: Tel.: + 86-731-88822829; Fax: +86-731-88823701.  
E-mail address: zgming@hnu.edu.cn (G. Zeng), A.Chen@hunau.edu.cn (A. Chen).

<sup>1</sup> These authors contribute equally to this article.

## Abstract

In this study, interaction of oxytetracycline (OTC) onto nano-hydroxyapatite (nHAP) was evaluated as affected by pH and metal ions. Results showed that the adsorption process of OTC was highly pH- and metallic species-dependent. The amount of sorbed OTC at four pH were in the order of pH 8.0 > pH 10.0 > pH 5.5 > pH 3.0 and reached equilibrium around 120 min, indicating adsorption affinity of four species to nHAP followed the order of  $\text{OTC}^- > \text{OTC}^{2-} > \text{OTC}^\pm > \text{OTC}^+$ . Adding metal ions greatly increased the distribution coefficient ( $K_d$ ) of OTC between adsorbents and aqueous phases, following the order of  $\text{Fe}^{3+} > \text{Cu}^{2+} > \text{Pb}^{2+} > \text{Cd}^{2+} = \text{Ca}^{2+}$  in the pH range of 3.0-10.0. Moreover, the co-adsorption behavior of OTC and heavy metals onto nHAP was also explored at pH 5.5 for the first time. OTC adsorption was significantly enhanced with the co-existence of 0.25 mmol/L  $\text{Cu}^{2+}$  or  $\text{Pb}^{2+}$ . Inversely, the presence of 0.25 mmol/L OTC slightly led to the improvement of  $\text{Cu}^{2+}$  adsorption and depression of  $\text{Pb}^{2+}$  adsorption, yet  $\text{Pb}^{2+}$  adsorption was obviously promoted with the co-existence of 0.25 mmol/L OTC. Meanwhile, adsorption of OTC and  $\text{Cd}^{2+}$  showed unapparent variation in single or binary systems. The bridging effect involving metal ions, O- and N- containing groups in OTC molecules, and  $\equiv\text{CaOH}$  or  $\equiv\text{POH}$  sites of nHAP resulted in the formation of ternary complexes which were responsible for the promotion of their adsorption, while dissolution-precipitation was another key mechanism with the co-existence of  $\text{Pb}^{2+}$ .

## Key words

Oxytetracycline; Metal ions; Nano-hydroxyapatite; Ternary complexation; Adsorption

mechanism.

## 1. Introduction

Tetracycline antibiotics (TCs) are extensively applied to improve livestock growth as veterinary medicine and prevent infectious diseases in modern healthcare [1, 2]. In 2011, the total usage of TCs is  $9.7 \times 10^7$  kg in China, accounting for 46% of all antibiotics [3]. Due to their poor absorption and metabolism *in vivo*, TCs may be directly transmitted into environment through feces and urine as active ingredients [4, 5]. To date, TCs as micro-pollutants have been found in various environmental mediums at the concentrations around 0.13-0.51  $\mu\text{g/L}$  in surface water, 86-199  $\mu\text{g/kg}$  in soils, and 4.58 mg/kg in animal dung samples [6-8]. The potential effects of TCs on organisms mainly including damage ecosystem functions and productivity, induce antibiotics resistance genes (ARGs) and increase adventure of antibiotic resistance gene transfer to human body through food chain [9-12]. Therefore, it is urgent to explore their environmental behaviors and efficient removal techniques.

Oxytetracycline (OTC) which belongs to the member of TCs, is a complicated molecule with multiple ionizable functional groups. Owing to the presence of amine groups and acid/base-active phenolic hydroxyl groups, OTC can undergo protonation-deprotonation reactions, thereby generating four species such as  $\text{OTC}^+$ ,  $\text{OTC}^\pm$ ,  $\text{OTC}^-$ , and  $\text{OTC}^{2-}$  under different pH. However, these species show high persistence and good solubility in water, leading to inability to completely removal from sewage in wastewater treatment plants (WWTP) [13-17]. What's more, metal ions such as zinc and copper are frequently applied as growth promoter along with

65 TCs in swine diets, which will induce co-contamination in the environment [18-22].  
 66 Specifically, TCs have different affinities to complex with diverse metal ions (e.g.  
 67  $\text{Cu}^{2+}$ ,  $\text{Ca}^{2+}$ ,  $\text{Fe}^{3+}$ ,  $\text{Cd}^{2+}$ , and  $\text{Pb}^{2+}$ ) to form metal ion-TCs pollutants due to the multiple  
 68 N- and O-containing moieties [23-25], which may affect their environmental  
 69 behaviors, including photodegradation [10, 26], redox reactions [7, 27], toxicity [28],  
 70 and adsorption [29]. Moreover, numerous literatures have reported that it is more  
 71 difficult to dislodge these co-pollutants from wastewater compared with that of single  
 72 pollutant [10, 30]. Although all kinds of approaches have been applied to remove  
 73 heavy metals or antibiotics from water, only adsorption is considered as an effective  
 74 and environment-protecting separation process for simultaneous removal of them  
 75 [29-32]. Among common adsorbents such as carbon nanotube [1], clay minerals [33],  
 76 biochar [29], mesoporous silica [31], and graphene oxide [34], minerals have been  
 77 frequently used as green adsorbents to treat wastewater containing heavy metals and  
 78 organic pollutants due to availability, low-cost, and high-efficiency [33]. Recent  
 79 studies also proved that the complexation between heavy metals and antibiotics could  
 80 promote the retention of them onto minerals and soils. For example, Gu et al. reported  
 81 that  $\text{Cu}^{2+}$  significantly increased the adsorption of ciprofloxacin (CIP) on goethite via  
 82 forming goethite- $\text{Cu}^{2+}$ -CIP surface complex at pH 6.0 [35]. Wang et al. found that the  
 83 TC- $\text{Cu}^{2+}$  complexes ( $\text{CuH}_2\text{TC}^{2+}$ ,  $\text{CuHTC}^+$ , and  $\text{CuTC}$ ) had higher sorption coefficient  
 84 ( $K_d$ ) onto montmorillonite than their corresponding TC species ( $\text{H}_3\text{TC}^+$ ,  $\text{H}_2\text{TC}$ , and  
 85  $\text{HTC}^-$ ) in the normal pH condition [36]. Further research suggested that the presence  
 86 of heavy metals enhanced the adsorption of TC on soils through an ion bridging effect

in the order of  $\text{Cu}^{2+} > \text{Pb}^{2+} > \text{Cd}^{2+}$  at pH 3.0-10.0. Conversely, the presence of TC had little effect on the adsorption of heavy metals [24]. Although these minerals exhibited good performance in the removal of antibiotics with the maximum adsorption capacity around 20-200 mmol/kg, the adsorption of heavy metals always remained at a low level with the co-existing of antibiotics. Thus, it is necessary to seek a mineral with high adsorption capacity towards heavy metals for enhancing OTC removal.

Nano-hydroxyapatite ( $\text{Ca}_{10}(\text{PO}_4)_6(\text{OH})_2$ , nHAP), a universal inorganic secondary metal minerals, was widely exploited in environmental remediation, novel bone-related scaffolds, and sustained drug release systems [37]. Over the past decades, it has been used as a mature stabilizer for removing heavy metals. Metal ions (e.g.  $\text{Cu}^{2+}$ ,  $\text{Pb}^{2+}$ ,  $\text{Cd}^{2+}$ ,  $\text{Zn}^{2+}$ , and  $\text{Co}^{2+}$ ) were successfully immobilized in wastewater and contaminated soil through interaction with nHAP to form composite phosphate [38]. Owing to the reaction sites (e.g.,  $\equiv\text{CaOH}$ ,  $\equiv\text{POH}$ ,  $\equiv\text{CaOH}^{2+}$ , and  $\equiv\text{PO}_3\text{H}^-$ ) on the surface of nHAP [14], it has been gradually used to get rid of the single pollution of antibiotics in water and soil. For example, Cazalbou et al. found that the maximum sorption capacity of TC onto biomimetic apatite was 70 mmol/kg at pH 7.4 [39]. Maria Harja et al. reported that the maximum removal efficiency of OTC by uncalcined nHAP was 97.6% at pH 8.0 within 60 min when the initial concentration was 100 mmol/kg [14]. Moreover, Li et al. fabricated a newly Fe-nHAP to dramatically enhance its removal efficiency for TC according to strong affinity between  $\text{Fe}^{3+}$  and OTC [40]. However, there is still a dearth of knowledge regarding whether nHAP is a promising candidate to control the combined pollution of

antibiotics and heavy metals in environmental remediation. To best of our knowledge, the adsorption process of OTC in the nHAP-OTC/heavy metals binary system has not been investigated until now. Therefore, it is well worth comprehensively exploring the co-adsorption behavior of OTC and heavy metals onto nHAP.

In this work, the objectives were to investigate (1) the adsorption behavior of OTC onto nHAP at four selected pHs; (2) effect of co-existing ions on the interaction between OTC and nHAP within pH 3.0-10.0; (3) sorption of OTC and heavy metals ( $\text{Cu}^{2+}$ ,  $\text{Cd}^{2+}$ , and  $\text{Pb}^{2+}$ ) onto nHAP in single or binary systems; and (4) the major interaction mechanisms among OTC, heavy metals and nHAP.

## 2. Materials and methods

### 2.1 Materials

Hydrochloride salt of OTC ( $\text{C}_{22}\text{H}_{24}\text{N}_2\text{O}_6 \cdot \text{HCl}$ , > 95% purity) was purchased from yuanye Bio-Technology Co., Ltd. (Shanghai, China). Methanol and acetonitrile were HPLC grade and obtained from Anaqua Chemicals Supply (ACS, USA). Other reagents, including sodium salts, nitrates, ammonium phosphate, sodium hydroxide, and nitric acid, were all purchased from Sinopharm Chemical Reagent Co. (China). Ultrapure water (resistance = 18.25  $\text{M}\Omega/\text{cm}$ ) was used throughout the experiment. Antibiotic stock solution was stored in dark at 4 °C for no long than three days.

### 2.2. Synthesis and characterization of nHAP

The synthesis process of nHAP was based on a modified method [14, 40]. Firstly, two starting solutions were prepared: dissolved the  $\text{Ca}(\text{NO}_3)_2 \cdot 4\text{H}_2\text{O}$  and  $(\text{NH}_4)_2\text{HPO}_4$  into the ultrapure water to achieve the solutions of 100 mmol/L  $\text{Ca}^{2+}$  and 100 mmol/L

131  $\text{PO}_4^{3-}$ , respectively. Under the magnetic stirring at 1000 rpm, 250 mL of 100 mmol/L  
132  $\text{Ca}^{2+}$  was dropwise added into 150mL of 100 mmol/L  $\text{PO}_4^{3-}$  using constant flow pump  
133 under appropriate fluid velocity for 1 h at  $60 \pm 1$  °C. During the reaction, the pH of  
134 the suspension was monitored and adjusted to  $11 \pm 0.5$  by NaOH solution (1 mol/L).  
135 Later, the suspension was left to mature for another 3 h at  $60 \pm 1$  °C. Finally, the  
136 obtained precipitate was filtered through a 0.22  $\mu\text{m}$  membrane, washed with ultrapure  
137 water for several times, and dried in the oven at 100 °C for 24h.

138 The hydrodynamic diameter of nHAP was measured by dynamic light scattering  
139 (DLS). The morphology and composition of nHAP were obtained by a field emission  
140 scanning electron microscope equipped with an EDAX attachment (FESEM:  
141 JSM-6700F, JEOL, Japan). The specific surface area of nHAP was determined by  
142 Brunauer-Emmentt-Teller (BET) with  $\text{N}_2$  adsorption and desorption isotherms at 77K.  
143 The crystalline structure of nHAP was characterized by an X-ray powder  
144 diffractometer (XRD) with monochromated Cu  $\text{K}\alpha$  ( $\lambda = 1.5418$  Å) radiation. Fourier  
145 transform infrared spectra of nHAP were recorded by the KBr pellet technique using a  
146 Nicolet Nexus 670 spectrophotometer (FTIR, Japan) in range of 4000-400 $\text{cm}^{-1}$ . X-ray  
147 photoelectron spectroscopy (XPS) analysis of nHAP was collected on an ESCALAB  
148 250Xi spectrometer (Thermo Fisher, USA).

### 149 2.3. Adsorption experiments

150 Batch experiments were agitated with a speed of 160 rpm for 12 h at 25 °C,  
151 and all solutions were wrapped with foil to eliminate photodegradation [41]. The  
152 adsorbent dosage was 1 g/L. Prior to addition of nHAP, solution pH was adjusted to

required value by adding negligible volumes of diluted NaOH or HCl solutions, and the final pH values were also measured. All data were recorded as the average of three duplicate experiments.

To investigate the influence of solution pH on adsorptive behaviors (kinetics and isotherms) of OTC onto nHAP, two types of adsorption experiment were carried out at pH 3.0, 5.5, 8.0, and 10.0. For kinetic experiments, 100 mg of nHAP was mixed with 100 mL OTC solution with 0.1 mmol/L of initial concentration. Time intervals of 5, 15, 30, 60, 90, 120, 150, and 180 min were selected as sampling points. For isotherm experiments, 30 mg of nHAP was added into 30 mL OTC solution with different concentrations of 0.02-0.24 mmol/L.

To reveal both co-existing ions and solution pH effects on OTC adsorption, 30 mL mixture of 0.1 mmol/L OTC with different concentrations of co-existing ions (0.25 mmol/L cations:  $\text{Na}^+$ ,  $\text{Ca}^{2+}$ ,  $\text{Fe}^{3+}$ ,  $\text{Cu}^{2+}$ ,  $\text{Pb}^{2+}$ , and  $\text{Cd}^{2+}$ ; 0.5 mmol/L anions:  $\text{NO}_3^-$ ,  $\text{Cl}^-$ ,  $\text{F}^-$ ,  $\text{CO}_3^{2-}$ ,  $\text{SO}_4^{2-}$ , and  $\text{PO}_4^{3-}$ ) were pre-equilibrated for 3 h at pH 3.0-10.0, and 0.1 mmol/L  $\text{NaNO}_3$  was set to the control group. Sorption isotherms of both OTC and heavy metals ( $\text{Cd}^{2+}$ ,  $\text{Cu}^{2+}$ ,  $\text{Pb}^{2+}$ ) onto nHAP in single or binary systems were also studied. The mixture with pH value of 5.5 was prepared as describe above, but 30 mL mixture were contained: (1) the OTC at initial concentrations of 0.02-0.24 mmol/L with 0, 0.1 and 0.25 mmol/L heavy metals; (2) the heavy metals at initial concentrations of 0.6-2.1 mmol/L with 0, 0.1 and 0.25 mmol/L OTC. Other operations were consistent with isotherm experiment of OTC.

After adsorption, 4 mL of aliquots were taken from suspension at the set time,

and quickly filtered using 0.45  $\mu\text{m}$  of membrane. The aqueous OTC was determined by a high performance liquid chromatography (HPLC, Agilent 1100) on a column of Zorbax Eclipse XDB-C 18 (150 $\times$ 4.6 nm, 5  $\mu\text{m}$ ) [24, 42]. The aqueous heavy metals were diluted with 4 mL  $\text{HNO}_3$  (5%) for inductively couple plasma optical emission spectroscopic analysis (ICP-OES, optima 5300 DV) [43, 44]. The adsorption capacity of OTC or heavy metals ( $q_e$ , mmol/kg) and distribution coefficients of OTC ( $K_d$ , L/kg) were calculated by expressing in Eqs. (1) and (2), respectively.

$$q_e = (C_o - C_e)V/m \quad (1)$$

$$K_d = q_e/C_e \quad (2)$$

Where  $C_o$  and  $C_e$  (mmol/L) are the initial and equilibrium concentrations of adsorbate, respectively;  $V$  (L) is the volume of solution and  $m$  (kg) is the mass of the adsorbent.

## 2.4 Spectroscopic measurements

The structure transformation of OTC arising from the complexation with metal ions was assessed by UV-vis absorption spectra. Above all, 0.1 mmol/L OTC was mixed with an equal volume of 0.1 mmol/L metal ions ( $\text{Na}^+$ ,  $\text{Ca}^{2+}$ ,  $\text{Fe}^{3+}$ ,  $\text{Cu}^{2+}$ ,  $\text{Pb}^{2+}$ , and  $\text{Cd}^{2+}$ ) under pH 4.0, 5.5, and 8.0. Then, 30 mL of mixture was pre-equilibrated for 3 h as above mentioned, the UV-vis spectra of mixture were quickly determined in the 220-500 nm range with a wavelength resolution of  $\Delta\lambda = 1$  nm.

## 2.5. Data analysis

In order to calculate the potential rate-controlling of the adsorption kinetics, the data were fitted with pseudo-first-order (PFO) (Eq. (3)), pseudo-second-order (PSO) (Eq. (4)), Elovich model (Eq. (5)) and intraparticle diffusion model (Eq. (6)), which

are represented as follows:

$$q_t = q_e(1 - \exp(-k_1 t)) \quad (3)$$

$$q_t = k_2 q_e^2 t / (1 + k_2 q_e t) \quad (4)$$

$$q_t = \ln(\alpha \beta t + 1) / \beta \quad (5)$$

$$q_t = k_{id} t^{0.5} + c \quad (6)$$

Where  $q_t$  (mmol/kg) and  $q_e$  (mmol/kg) represent the adsorption capacity of adsorbent at time  $t$  (min) and equilibrium time, respectively;  $k_1$  (1/min) and  $k_2$  (kg/(mmol min)) are rate constant of PFO and PSO, respectively;  $\alpha$  (mmol/kg min) and  $\beta$  (kg/mmol) are initial rate constant of chemisorption and constant of surface coverage and activation energy in Elovich equation, respectively;  $k_{id}$  (mmol/kg min<sup>0.5</sup>) is the intraparticle diffusion rate constant and  $c$  (mmol/kg) is a constant of the boundary layer thickness;  $t$  (min) is contact time.

The Langmuir (Eq. (7)) and Freundlich (Eq. (8)) models were applied to describe the equilibrium nature of CTC and heavy metals onto nHAP at different conditions, respectively. The equations are as follows:

$$q_e = q_{max} b C_e / (1 + b C_e) \quad (7)$$

$$q_e = K_f C_e^n \quad (8)$$

Where  $q_e$  (mmol/kg) represents the adsorption capacity of adsorbent at equilibrium;  $C_e$  (mmol/L) is the equilibrium concentrations of adsorbate;  $q_{max}$  (mmol/kg) and  $b$  (L/mmol) are the Langmuir model adsorption parameters, where  $q_{max}$  represents the maximum sorption capacity of adsorbate onto adsorbent, and  $b$  is related to sorption affinity.  $K_f$  (mmol<sup>1-n</sup>L<sup>n</sup>/kg) and  $n$  are the Freundlich model adsorption parameter,

where  $K_f$  relates to adsorption capacity, and  $n$  is the empirical constant associated with adsorption intensity.

The Chi-square test ( $\chi^2$ ) and the coefficient of determination ( $R^2$ ) were also used in order to further evaluate the reliability of various models, where smaller  $\chi^2$  and higher  $R^2$  value implied a better fitting of model with the experimental data [45]. All parameters in the equation were derived from the stimulation of OriginLab 8.0 software.

### 3. Results and discussion

#### 3.1 Characterization of the sorbents

The morphology and composition of nHAP were characterized by FESEM and EDAX, respectively. As seen in Fig. 1A, the FESEM image indicates that the nHAP is needle-like shape, 20-50 nm in diameter and 100-200 nm in length. Due to aggregation, the structure of nHAP shows stacked and irregular surfaces with intergranular porosity. Fig. 1B shows that the hydrodynamic diameter of nHAP in suspension is 147.8 nm after pretreating by ultrasound. The main reasons why an overestimated diameter was measured in DLS analysis compared with that in FESEM was that the DLS analysis was conducted with the sample in the hydrated state, while in the FESEM the estimated size was performed in the solid state [46]. The corresponding EDAX spectrum of native nHAP in Fig. 1C demonstrates that the Ca/P molar ratio is 1.63 in the presence of calcium, phosphorus and oxygen, which proves the composition of sample as hydroxyapatite. Besides, Fig. 1D displays the full  $N_2$  adsorption-desorption isotherms and the pore distribution curve for nHAP. The BET

surface area and the total pore volume of nHAP are 55.24 m<sup>2</sup>/g and 0.19 cm<sup>3</sup>/g, respectively. On the basis of IUPAC classification, nHAP possesses a type IV isotherms with a hysteresis loop at approximately  $P/P_0 = 0.83-0.99$ , implying the characteristics of mesoporous materials [47]. The pore size distribution curve obtained by the desorption branch of the isotherms based on BJH model is also inserted in Fig. 1D. It can be seen that the size of pores are centered at 30 nm and not evenly distributed on the whole. The phase purity of nHAP was also analyzed by XRD. From Fig. 2A, the XRD diffraction peaks of nHAP are well indexed to the reference JCPDS file number (NO.09-0423) [48].

The FT-IR spectra of OTC and nHAP are presented in Fig. 2B. In the FT-IR spectrum of OTC, the broad band between 3600 cm<sup>-1</sup> and 3000 cm<sup>-1</sup> were attributed to the H-bonded hydroxyl groups in phenolic and alcoholic groups. The peaks at 1669 cm<sup>-1</sup> and 1528 cm<sup>-1</sup> belonged to the skeletal vibration of C=O at C<sub>2</sub> site and =NH<sub>2</sub> at N<sub>2a</sub> site in ring A (seen in Fig. 5A). The peaks at 1615 cm<sup>-1</sup> and 1582 cm<sup>-1</sup> were attributed to C=O at C<sub>1</sub> site in ring C and =NH at N<sub>4a</sub> site in ring A, respectively, while the peak at 1457 cm<sup>-1</sup> was assigned to C=C skeletal vibration. In the FT-IR spectrum of nHAP, the characteristic band around 3567cm<sup>-1</sup> and the peak at 3446 cm<sup>-1</sup> were attributed to O-H group hosted by the adsorbed water and nHAP framework, respectively [40]. The peak at 1093 cm<sup>-1</sup> or 1035 cm<sup>-1</sup> and the peak at 605 cm<sup>-1</sup> or 565 cm<sup>-1</sup> were relevant to asymmetrical stretching and bending modes of PO<sub>4</sub><sup>3-</sup> ions, respectively. Meanwhile, the peak at 962 cm<sup>-1</sup> was attributed to symmetric stretching mode of the PO<sub>4</sub><sup>3-</sup> ions [49]. Due to the presence of HPO<sub>4</sub><sup>2-</sup>, a small peak at 874 cm<sup>-1</sup>

was also detected.

### 3.2 Kinetics of OTC adsorption

The adsorption kinetic plotted in Fig. 3A as adsorption capacities vs contact time is nonlinear. It is noteworthy that the curves under different solution pH exhibit the similar trend. OTC adsorption onto nHAP rapidly increased within the first 15 min due to the abundant adsorption sites. After 15 min, adsorption rate slowly decreased, and gradually reached equilibrium at 120 min.

To understand the time-dependent adsorption of OTC onto nHAP, PFO, PSO, Elovich and intraparticle diffusion models were applied to fit the experiment data. The kinetic parameters are presented in Table 1. PFO and PSO are considered to determine the rate-limiting step of the adsorption process at first. Compared with PFO, the smaller  $\chi^2$  (0.96-8.00) and higher  $R^2$  value (0.968-0.982) were found in PSO and the values of  $q_{e,cal}$  simulated by PSO were more close to the  $q_{e,exp}$  values, which implied that OTC sorption onto nHAP was uppermost controlled by chemisorption [50, 51]. The results of PSO rate constant  $K_2$  (kg/mmol min) and the initial adsorption rate  $h$  ( $K_2q_e^2$ , mmol/kg min), greatly impacted by the species distribution of OTC, were noted as 0.0049-0.0094 kg/mmol min and 4.19-14.76 mmol/kg min, respectively. The initial adsorption rates under four pH values followed an order of pH 8.0 > pH 10.0 > pH 5.5 > pH 3.0, indicating that adsorption affinity of different species followed the order as:  $OTC^- > OTC^{2-} > OTC^\pm > OTC^+$ , especially at the beginning of the adsorption process [52]. However, previous studies pointed out that the idea to restrict the fit to only PFO and PSO was unsupported since the adsorption process often took

place in complicated adsorbate/adsorbent systems, including often complex molecules, sometimes heterogeneous surface [39]. Therefore, Elovich model, identified as the best-fitted (highest  $R^2$  ( $> 0.990$ ) and lowest  $\chi^2$  (0.23-1.03)) model, was chosen to further illustrate reaction mechanism. In combination with the assumption of this model, we concluded that OTC molecules were primarily adsorbed onto the heterogeneous sites of nHAP via chemical action.

Since the above kinetic models were unable to describe the mass transfer steps in OTC adsorption, intraparticle diffusion model was further fitted in Fig. 3B. As seen, the plot of this model was multi-linear containing three distinct parts. The first stage (first 15 min) with the steepest segment was mainly ascribed to the transfer of OTC from liquid phase to the external surface of nHAP through film diffusion [53]. Due to the higher affinity of OTC<sup>-</sup> to nHAP, the maxima of  $k_{ld}$  (mmok/kg) was obtained at pH 8.0 in Table 1. The second stage (30-120 min) showed a gradual adsorption process controlled by intraparticle diffusion (from external surface into the pores of nHAP). In addition, the intraparticle diffusion started to reach saturation at the last stage (120-180 min) because of the decrease in the active sites for nHAP. Thus, we found that both film diffusion and intraparticle diffusion existed in the diffusion process. Furthermore, all of the linear plots did not pass through the origin, which also proved that intraparticle diffusion was not the sole rate-controlling step [45].

### 3.3 Isotherms of OTC adsorption

Two most prevailing isotherm models (Langmuir and Freundlich) were applied to analyze the data (Fig. 3C), and relevant parameters were calculated and listed in

Table 2. As shown in Table 2, Freundlich model presented higher  $R^2$  (0.982-0.991) and smaller  $\chi^2$  (0.10-6.22) compared with Langmuir model, implying that the adsorption of OTC on nHAP was heterogeneous with multilayer uptake. Besides, the  $n$  values (0.17-0.33) defined as heterogeneity factor is much less than 1, suggesting that adsorption sites on nHAP interact with OTC via weak free energies [50].

In generally, the adsorption capacity and adsorption mechanism are influenced by solution pH through changing both the surface chemistry of adsorbents and the ionization state of pollutant. The OTC's  $K_f$  varied from 33.34 to 139.38  $\text{mmol}^{1-n}\text{L}^n/\text{kg}$  (Table 2). It was obvious that  $K_f$  increased rapidly with increasing pH values from 3.0 to 8.0, and then marginally decreased with increasing pH values from 8.0 to 10.0. The trend kept similar pace with the pH-regulated distributions of OTC<sup>-</sup>. However, the adsorption capacity at pH 3.0 was about 4 times smaller than that at other pH values, mainly attribution to two aspects: (1) destruction of the embedding calcium triangles structure contributed to the interaction between hydroxyl group and hydroxide ions under acidic medium [32], resulting in the depression of both hydrogen bonding and complexation between nHAP and OTC, followed by the maximum fluctuation of solution pH from 3.0 to 6.5 in Fig. 3C; (2) when solution pH was under PZC of nHAP (6.5-7.0) [14], the surface charge of nHAP was positive and the major species of OTC are OTC<sup>+</sup> and OTC<sup>±</sup>, which might produce a lasting electrostatic repulsion on reaction interface. Combined with Figs. 3C and D, no matter how solution pH was changed between 5.5 and 10.0, the adsorption capacity always floated in a small range. Thus, nHAP is an outstanding adsorbent for coping with antibiotic wastewater at various pH

except for strong acidity. At  $\text{pH} > 7.0$ , the main types of OTC are  $\text{OTC}^-$ ,  $\text{OTC}^{2-}$ , and  $\text{OTC}^\pm$  with higher affinity to nHAP, but electrostatic repulsion is stronger than electrostatic attraction. We speculate that electrostatic forces should play a secondary role in adsorption process.

### 3.4 Metal ions – OTC interaction in solution

The interaction between OTC and metal ions was studied via spectroscopic measurements. UV-vis spectra and reaction mechanisms of OTC-metal complexes are shown in Fig.4 and Table 3. As shown in Fig. 4, different degrees of spectral redshifts were observed in mixed systems due to the significant intramolecular charge transfer between OTC and metal ions [29]. Literatures have reported that TCs' A ring chromophore contributed to the adsorption band at 250-300 nm, meanwhile the BCD ring chromophore contributed to the adsorption band at both 250-300 and 340-380 nm [7, 54]. It was pretty clear that the absorbance of  $\text{OTC-Fe}^{3+}$  complexes increased significantly around 250-300 nm within all pH values, but decreased slightly around 340-380 nm because of OTC's self-degradation accelerated by  $\text{Fe}^{3+}$  [7]. Thus,  $\text{Fe}^{3+}$  likely complexes with A ring at  $\text{O}_3\text{-O}_{2a}$  site when  $\text{O}_3$  atom becomes the first donor group, or at  $\text{N}_{4a}\text{-O}_{12a}$  site until the deprotonation of  $\text{C}_4$  dimethylammonium group, but shows no apparent impact on BCD ring (Table 3). Significant redshifts of  $\text{OTC-Cu}^{2+}$  complexes were found around both 250-300 and 340-380 nm except pH 3.0 (seen in Fig. 4A), in which the stability constant of  $\text{CuH}_2\text{OTC}^{2+}$  was under a lower level ( $\log K_{\text{Cu,OTC}} = 5.02$ ) at pH 3.0 so that UV-vis spectra could not detect the discernible ligand-to-metal charge transfer (LMCT). As discussed by Jezowska-Bojczuk and Jin

[10, 55], it could be inferred that O<sub>3</sub>-O<sub>2a</sub> site firstly bound with Cu<sup>2+</sup> at low pH, with CuH<sub>2</sub>OTC<sup>2+</sup> as the unstable species. When solution pH was raised, CuHOTC<sup>+</sup> or CuOTC<sup>±</sup> was preferentially substituted for CuH<sub>2</sub>OTC<sup>2+</sup>, and chelation then converted to the O<sub>11</sub>-O<sub>12</sub> site. If the ratio of copper ions to OTC was greater than 1, the O<sub>3</sub>-O<sub>2a</sub> site of CuHOTC<sup>+</sup> and the N<sub>4a</sub>-O<sub>12a</sub> site of CuOTC<sup>±</sup> might further bind with free copper ions to form 1:2 ligand-to-metal complexes, with Cu<sub>2</sub>HOTC<sup>3+</sup> and Cu<sub>2</sub>OTC<sup>2+</sup> as the ultimate species, respectively. For OTC-Pb<sup>2+</sup> complexes, their significant redshifts were only detected at 340-380 nm adsorption band under pH 8.0, suggesting that Pb<sup>2+</sup> could only complex at the O<sub>11</sub>-O<sub>12</sub> site in ring BCD, with PbOTC<sup>±</sup> as the unique complexes [56]. Based on Pearson's Hard-Soft Acid-Base (HSAB) theory [57], ligands such as phenolic-diketone group and tricarboxyl group in OTC molecule would be served as soft bases owing to their large ionic radius and strong polarizability of conjugated electron clouds. Hence, Lewis acids such as Fe<sup>3+</sup>, Cu<sup>2+</sup> and Pb<sup>2+</sup> could coordinate with these soft bases in antibiotics molecules.

Although complete overlap of absorbance and peak locations occurred in both OTC-Ca<sup>2+</sup> ( $K_{Ca,OTC} = 10^{6.44}$ ) complexes and OTC-Cd<sup>2+</sup> complexes ( $K_{Cd,OTC} = 10^{6.9}$ ) due to weak iron-chelation activity, the complexes like Ca<sub>2</sub>OTC<sup>2+</sup> and CdOTC<sup>±</sup>, were also found in previous literature [50, 58, 59]. For example, Ca<sup>2+</sup> chelated easily with OTC<sup>2-</sup> to form complexes with less protons through pH-metric titration analysis [58]. More specifically, Ca<sup>2+</sup> would bond with TC to form a 1:2 ligand-to-metal complex via chelation with O<sub>11</sub>-O<sub>12</sub> site resulting in the extended conformation A of TC, and then bound with OH<sub>12a</sub> and N<sub>4a</sub> sites through hydrogen bonding to relieve the steric

crowding [59]. Just like OTC-Pb<sup>2+</sup> complexes, Cd<sup>2+</sup> would also complex with O<sub>11</sub>-O<sub>12</sub> site of OTC<sup>2-</sup> to form a unstable complex, such as CdOTC<sup>±</sup> [50, 56].

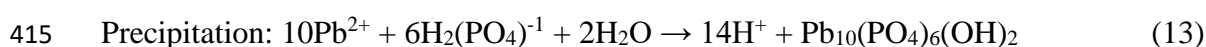
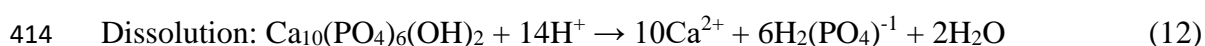
### 3.5 Effect of co-existing ions on OTC adsorption

The distribution coefficients ( $K_d$ , L/kg) of OTC were calculated in the presence of cations at 0.25 mmol/L or anions at 0.5 mmol/L with the solution pH values ranging from 3.0 to 10.0. The adsorption envelopes for OTC onto nHAP in the presence of co-existing ions were bell shaped in generally. As showed in Fig. 5B, the promotion in  $K_d$  influenced by the six cations had the order of Fe<sup>3+</sup> > Cu<sup>2+</sup> > Pb<sup>2+</sup> > Cd<sup>2+</sup> = Ca<sup>2+</sup> = Na<sup>+</sup>, which was highly dependent on their complexation ability with OTC. Xu et al. reported that the predominant surface sites in nHAP suspension were ≡POH at pH < PZC and ≡CaOH at pH > PZC, respectively, whereas ≡PO<sup>-</sup> and ≡CaOH<sub>2</sub><sup>+</sup> became significant at pH near PZC [60]. Thus, OTC could be adsorbed onto ≡CaOH<sub>2</sub><sup>+</sup> and ≡POH mainly via cationic exchanges with Ca<sup>2+</sup> and H<sup>+</sup> at pH < 7.0, and complex with ≡CaOH to form insoluble Ca<sub>2</sub>OTC<sup>2+</sup> and CaOTC<sup>±</sup> complexes at pH > 7.0. When Fe<sup>3+</sup> or Cu<sup>2+</sup> presented in the solution,  $K_d$  values were increased by two orders of magnitude at pH < 6.0, and then dropped dramatically at pH > 6.0. According to previous literatures [60, 61], with the co-existence of metal ions (Me<sup>n+</sup> represents Fe<sup>3+</sup>, Cu<sup>2+</sup>, Cd<sup>2+</sup>, and Pb<sup>2+</sup>), the following interactions may occur:



Therefore, Me<sup>n+</sup> could act as a bridge ion between OTC and nHAP to form insoluble

395 nHAP-Me-OTC ternary complexes, resulting in reinforcing the liquid-solid separation  
 396 of OTC from aqueous media. The influence of metal ions on OTC adsorption might  
 397 include three possible mechanisms: (1) 1:1 or 1:2 ligand-to-metal complexes had  
 398 stronger affinity with nHAP than either OTC species alone; (2) at pH < 7.0, metal ions  
 399 might be firstly adsorbed on surface sites via ion-exchange to form nHAP-Me while  
 400 part of OTC was also loaded on the surface through weak free energies, and then the  
 401 nHAP-Me further adsorbed OTC to form stability complexes due to stronger affinity.  
 402 (3) at pH > 7.0, the soluble complexes, such as  $\text{Cu}_2\text{HOTC}^{3+}$ ,  $\text{Cu}_2\text{OTC}^{2+}$  and  $\text{PbOTC}^+$ ,  
 403 could be captured onto the negatively charged surface of nHAP via electrostatic  
 404 attraction. In addition, the tendency of  $K_d$  may be greatly impacted by the solubility  
 405 product constant (e.g.  $K_{sp}(\text{Fe}^{3+}) = 4.0 \times 10^{-38}$ ;  $K_{sp}(\text{Cu}^{2+}) = 4.8 \times 10^{-20}$ ;  $K_{sp}(\text{Pb}^{2+}) =$   
 406  $1.0 \times 10^{-16}$ ), because the degree of metal precipitation is in an inverse ratio of  $K_{sp}$  value.  
 407 As the pH gradually changed from acidic to alkaline,  $\text{Me}^{n+}$  might gradually precipitate  
 408 to form  $\text{Me}(\text{OH})^{n+}$  in solution so that in turn impeded the promotion effect.  
 409 According to the study of Mavropoulos et al [61], only part of  $\text{Pb}^{2+}$  (20~30%) were  
 410 adsorbed on the surface by ion-exchange or complexation, and a two-stage  
 411 mechanism including nHAP dissolution and hydroxypyromorphite (HP) precipitation  
 412 was actually the controlling step for lead immobilization, which could be described by  
 413 following interactions:



416 After introduction into the reaction system, OTC molecules had more opportunities to

interact with the adsorption sites during nHAP dissolution, and then the relevant complexes including  $\text{Ca}_2\text{OTC}^{2+}$ ,  $\text{CaOTC}^\pm$ , and  $\text{PbOTC}^\pm$  might be sequestered into crystal lattice during HP precipitation and re-arranged to form solid solutions. As opposed to other systems,  $K_d$ 's tendency of nHAP-OTC/ $\text{Cd}^{2+}$  remained unchanged, which might be related to the similar stability constant compared with  $\text{Ca}^{2+}$ .

It is well-known that anions could not complex with OTC species. However,  $\text{SO}_4^{2-}$  and  $\text{CO}_3^{2-}$  would replace structural  $\text{PO}_4^{3-}$  to form  $\text{Ca}_{10}(\text{PO}_4,\text{SO}_4)_6(\text{OH})_2$  and  $\text{Ca}_{10}(\text{PO}_4,\text{CO}_3)_6(\text{OH})_2$ , respectively. Meanwhile  $\text{F}^-$  and  $\text{Cl}^-$  would isomorphous substitute for structural  $\text{OH}^-$  to form fluorapatite (FA,  $\text{Ca}_{10}(\text{PO}_4)_6\text{F}_2$ ) and chlorapatite (CA,  $\text{Ca}_{10}(\text{PO}_4)_6\text{Cl}_2$ ). As shown in Fig. 5C,  $K_d$  reduction for OTC adsorption generally followed an order of  $\text{PO}_4^{3-} > \text{SO}_4^{2-} > \text{CO}_3^{2-} = \text{F}^- > \text{Cl}^- > \text{NO}_3^-$ . This phenomenon was quite common in Hofmeister effect, both at interfaces and in solution medium [62]. In our case, the presence of  $\text{PO}_4^{3-}$  and  $\text{SO}_4^{2-}$  could significantly inhibit OTC adsorption, because  $\text{PO}_4^{3-}$  and  $\text{SO}_4^{2-}$  were easier to compete with OTC to approach superficial  $\text{Ca}^{2+}$  [52, 63], and then held back the formation of nHAP-OTC binary complexes, especially compared with anion species ( $\text{OTC}^-$  and  $\text{OTC}^{2-}$ ) at  $\text{pH} > 7.0$ . In contrast, the low-affinity ligands such as  $\text{CO}_3^{2-}$ ,  $\text{F}^-$  and  $\text{Cl}^-$  exerted a minor inhibition to OTC adsorption. It was likely that solution pH might occupy the leading status compared with the disturbance of the three anions.

### 3.6 Mutual effects of OTC and heavy metal on adsorption isotherms

Up to now, little is known about the influence of heavy metal on organics adsorption, and conversely organics, to heavy metal adsorption on apatite. Therefore,

nHAP was adopted as adsorbent to illuminate their mutual effects on adsorption isotherms. Adsorption isotherms of OTC and heavy metals in single or binary systems are shown in Fig. 6 and Fig. 7, respectively. Meanwhile the corresponding parameters calculated by Langmuir and Freundlich models are also listed in Table 2. No matter in single or binary systems, the adsorption of OTC onto nHAP was Freundlich type ( $R^2 > 0.98$ , and  $6.0 < \chi^2 < 44.0$ ), and the adsorption of heavy metals onto nHAP was Langmuir type ( $R^2 > 0.98$ , and  $20.0 < \chi^2 < 125.0$ ). Besides, the binary systems showed different adsorption performances by means of antagonistic, neutral and synergistic effects.

As shown in Figs. 6A and 7A, the addition of  $\text{Cu}^{2+}$  dramatically facilitated OTC adsorption on nHAP, and the presence of OTC also enhanced  $\text{Cu}^{2+}$  adsorption on nHAP with minor variation at pH 5.5, which indicated the synergistic effect on adsorption isotherms between OTC and  $\text{Cu}^{2+}$ . The similar phenomenon was found on goethite, montmorillonite, and mesoporous silica [35, 36, 64], showing discrepancy with biochar and chitosan [29, 65]. As shown in Table 4, the maximum Freundlich parameter ( $K_f$ ) of OTC onto nHAP was  $411.16 \text{ mmol}^{1-n} \text{L}^n / \text{kg}$  in the presence of  $\text{Cu}^{2+}$ , which was about 3.4 times than that in single system, with  $K_f$  value of  $120.96 \text{ mmol}^{1-n} \text{L}^n / \text{kg}$ . Conversely, the maximum sorption amount ( $q_{\max}$ ) of  $\text{Cu}^{2+}$  to nHAP was  $865.89 \text{ mmol/kg}$  in the presence of OTC, with an increase of 114.2% in  $q_{\max}$  values compared with single system. Despite this, the  $n$  values of OTC (Freundlich fit) in binary systems were smaller than those in OTC alone system, but the  $b$  values of  $\text{Cu}^{2+}$  (Langmuir fit) in binary systems were larger than those in  $\text{Cu}^{2+}$  alone system. The

above comparison revealed that the OTC-Cu<sup>2+</sup> complexes (e.g. CuOTC<sup>0</sup> and CuHOTC<sup>+</sup>) would have higher affinity to nHAP than OTC and Cu<sup>2+</sup> separately.

Unlike Cu<sup>2+</sup>, although the addition of Pb<sup>2+</sup> also considerably enhanced OTC adsorption on nHAP with  $K_f$  values ranging from 120.96 to 233.80 mmol<sup>1-n</sup>L<sup>n</sup>/kg, opposite behaviors for Pb<sup>2+</sup> adsorption were found in the presence of OTC, involving an increase of 28.1% at 0.10 mmol/L OTC and an decrease of 12.6% at 0.25 mmol/L OTC, respectively (Figs. 6B and 7B). Due to the special mechanism of lead immobilization by nHAP, the process was similar to co-precipitation of dissolved organic matter (DOM) and metal ions with Fe in many environments [66]. Besides, the promotion or inhibition for lead immobilization really depends on the concentration of OTC. The addition of 0.10 mmol/L OTC could complex with Pb<sup>2+</sup> to form PbOTC<sup>0</sup> with higher affinity to nHAP, and the new precipitate might have larger surface area and newly formed binding sites due to OTC/Pb<sup>2+</sup> loading, implying the promotion effect on removal of both Pb<sup>2+</sup> and OTC. When OTC concentration reached to 0.25 mmol/L,  $\equiv\text{FeOPb}^{2+}$  and  $\equiv\text{CaOPb}^{2+}$  on the surface were probably saturated with regard to OTC loading, and an increasing amount of OTC might blockade the metal sites due to the formation of organic multilayers, which resulted in ending the reactions of (12) and (13) at the early stage [61, 66, 67]. Either way, the adsorption processes of both OTC and Cd<sup>2+</sup> were always independent in binary systems, which suggested the neutral effect on adsorption isotherms between OTC and Cd<sup>2+</sup> (Figs. 6C and 7C).

### 3.7 Adsorption mechanism

XPS, FTIR and XRD analyses were performed to understand the interaction mechanism about adsorption of both OTC and metal ions onto nHAP. The results of XPS survey scans of seven samples are shown in Fig. 8A. Obviously, the major elements including Ca, P and O were found on the surfaces of these samples. The minor peaks of N 1s, Fe 2p, Cd 3d, Cu 2p and Pb 4f provided evidence of metal ion-OTC interactions on nHAP. More explanations are given below:

The Ca 2p XPS spectra are shown in Fig. 8B. Two peaks located at 350.68 and 347.11 eV were assigned to Ca 2p<sub>1/2</sub> and Ca 2p<sub>3/2</sub>, respectively [52]. The binding energy of Ca 2p<sub>3/2</sub> in nHAP increased from 347.11 to 347.45 eV after OTC loading, which was attributed to the interaction between OTC and ≡CaOH. When OTC and metal ions coexisted in the aqueous solution, the binding energy of Ca 2p of these samples changed slightly as compared with nHAP-OTC, since OTC exhibited higher affinity toward Fe<sup>3+</sup>, Cu<sup>2+</sup> and Pb<sup>2+</sup> compared with Ca<sup>2+</sup>. The high resolution XPS spectra of Fe 2p and Cu 2p are also shown in Figs. 8C and D. It was obvious that the XPS spectra of Fe 2p could be divided into six peaks, including Fe<sup>2+</sup> 2p<sub>3/2</sub> peak at 710.26 eV, Fe<sup>3+</sup> 2p<sub>3/2</sub> peak at 712.26 eV, Fe<sup>2+</sup> 2p<sub>1/2</sub> peak at 723.75 eV, Fe<sup>3+</sup> 2p<sub>1/2</sub> peak at 726.54 eV, and two satellite peaks at 716.29 and 719.71 eV, indicating that Fe existed as Fe<sup>2+</sup> and Fe<sup>3+</sup> in the samples and coordinated with nHAP to form Fe-O bond. Besides, the peak of Fe<sup>3+</sup> 2p<sub>3/2</sub> shifted from 712.26 eV to 713.64 eV after OTC loading because of the interaction between Fe<sup>3+</sup> and OTC [31]. In the Cu 2p spectra, two peaks located at 952.70 and 932.90 eV were assigned to the Cu 2p<sub>1/2</sub> and Cu 2p<sub>3/2</sub>, respectively [68]. The peak of Cu 2p<sub>3/2</sub> shifted from 932.90 to 933.31 eV after OTC

loading. Moreover, a new minor peak of Cu 2p<sub>3/2</sub> was observed at 934.81 eV, which might be attributed to the interaction of Cu<sup>2+</sup> with the amino groups in OTC molecules to form stable complexes [34].

As for O 1s spectra in Fig. 9, three peaks located at 532.51, 531.18 and 530.59 eV were corresponded to 16.43% of chemisorbed H<sub>2</sub>O, 48.88 % of hydroxyl groups on nHAP surface (e.g. ≡CaOH and ≡POH), and 34.69% of metallic oxide as well as phosphorus oxide (M-O), respectively. When OTC was absorbed on nHAP, the area ratio of hydroxyl groups reduced from 48.88% to 44.44%, indicating that hydroxyl groups played an important role in OTC adsorption onto nHAP. Correspondingly, the increased ratio of M-O from 34.69% at 530.59 eV to 39.17% at 530.66 eV was assigned to the formation of Ca-O between ≡CaOH and OTC (Fig 9B). Besides, the area ratio of M-O dramatically increased from 34.69% to 54.65%, 50.05%, and 49.63% after OTC/Fe<sup>3+</sup>, OTC/Cd<sup>2+</sup>, and OTC/Cu<sup>2+</sup> loading, respectively, and the area ratio of hydroxyl groups also reduced proportionally (Figs. 9. (D-G)). These changes might be ascribed to (1) the formation of ≡POMe<sup>(n-1)+</sup> and ≡CaOMe<sup>(n-1)+</sup> via the interaction shown in eqs. (9), (10), and (11) after metal ions loading; (2) the formation of ternary complexes, such as nHAP-Cu-OTC and nHAP-Pb-OTC, in which Cu<sup>2+</sup> or Pb<sup>2+</sup> could interact with O-containing groups in OTC molecules according to the proposed binding sites in Table 3.

According to FT-IR spectra (Fig.2B), the characteristic peaks of OTC were detected in HAP-OTC spectrum at the region of 1700-1400 cm<sup>-1</sup>, such as 1651, 1610 and 1458 cm<sup>-1</sup>. It was likely that the peak belonged to C=O at C<sub>2</sub> site in ring A shifted

from 1669 to 1651  $\text{cm}^{-1}$  due to hydrogen bonding of  $\equiv\text{POH}$  and complexation with  $\text{Ca}^{2+}$  species [40]. The peak belonged to  $\text{C}=\text{O}$  at  $\text{C}_{11}$  site in ring C became blunter and slightly shifted from 1615 to 1610  $\text{cm}^{-1}$  and the peak at 1582  $\text{cm}^{-1}$  belonging to  $=\text{NH}$  at  $\text{N}_{4a}$  site in ring A almost disappeared, which might be explained by complexation with  $\text{Ca}^{2+}$  ions on the surface of adsorbent. Compared with nHAP-OTC, the FT-IR spectra of nHAP-OTC/ $\text{Cd}^{2+}$  stayed the same after OTC/ $\text{Cd}^{2+}$  loading. While the peak located at 1669  $\text{cm}^{-1}$  sharply shifted to 1646  $\text{cm}^{-1}$  in nHAP-OTC/ $\text{Fe}^{3+}$  spectra because of the strong complexation of  $\text{Fe}^{3+}$  with  $\text{O}_3\text{-O}_{2a}$  site in OTC molecule. Moreover, the peaks of  $\text{C}=\text{O}$  groups located at 1651 and 1610  $\text{cm}^{-1}$  shifted to 1655 and 1600  $\text{cm}^{-1}$  in nHAP-OTC/ $\text{Cu}^{2+}$  spectra, respectively, testifying the chelating path of  $\text{Cu}_2\text{HOTC}^{3+}$  in Table 3. On the whole, the peak area of OH between 3600 and 3400  $\text{cm}^{-1}$  dramatically decreased after the reactions, which was consistent with XPS analysis. Besides, the  $\text{C}=\text{C}$  skeletal vibration at 1457  $\text{cm}^{-1}$  was no lateral movement, but the peak area of this band decreased in these systems, possibly resulting from the reduction of carbon density after loading on nHAP.

Interestingly, Additional peaks ( $21.6^\circ$  and  $30.2^\circ$ ) were found and identified as  $\text{Pb}_{(10-x)}\text{Ca}_x(\text{PO}_4)_6(\text{OH})_2$  in the nHAP-OTC/ $\text{Pb}^{2+}$ , but the XRD patterns of other samples kept unchanged in Fig. 2A, which indicated that the reaction between OTC/ $\text{Pb}^{2+}$  and nHAP was involved into mineral interior via a mechanism of dissolution and precipitation. Although a part of nHAP could react with OTC/ $\text{Pb}^{2+}$  to produce HP-OTC deposits according to reactions of (12) and (13), nHAP-Pb-OTC might also form on the surface of nHAP via an ion bridge effect. Specifically, the

peak located at  $1610\text{ cm}^{-1}$  shifted to  $1598\text{ cm}^{-1}$  in nHAP-OTC/ $\text{Pb}^{2+}$  spectra due to the complexation of  $\text{Pb}^{2+}$  with C=O at  $\text{C}_{11}$  in OTC molecules (Fig. 2B), which could verify the possibility of OTC adsorption on nHAP-Pb. Therefore, the interaction among OTC,  $\text{Pb}^{2+}$  and nHAP was co-determined by dissolution-precipitation mechanism and bridging effects.

#### 4. Conclusions

In summary, the interaction of OTC onto nHAP was influenced by OTC species under pH-regulation, complexing affinity of metal ions, and the process of co-precipitation in lead immobilization. The results implied that adsorptions of OTC were fitted by Elovich and Freundlich models, and adsorptions of heavy metals were described by Langmuir model. Anion species exhibited strong adsorption affinity at  $\text{pH} = 8.0$  and high contribution to the overall adsorption of OTC. Besides, the presence of metal ions enhanced OTC adsorption via an ion bridge effect. When OTC and  $\text{Cu}^{2+}$  co-existed in the solution, the adsorption of both OTC and  $\text{Cu}^{2+}$  on nHAP were improved due to the stronger affinity of OTC- $\text{Cu}^{2+}$  complexes compared with sole OTC or  $\text{Cu}^{2+}$ . Meanwhile the interactions between  $\text{Cd}^{2+}$  and OTC were too feeble to exhibit significant changes in binary system resulting in the independent sorption of both OTC and  $\text{Cd}^{2+}$ . However, the adsorption of OTC and  $\text{Pb}^{2+}$  onto nHAP was different from other systems since the interaction among OTC,  $\text{Pb}^{2+}$  and nHAP was co-determined by dissolution-precipitation mechanism and bridging effects. These findings not only help us understand how pH and metal ions influence OTC

migration and transformation in the environment, but also prove the potential application of nHAP to remediate the co-contamination of them in environment.

## Acknowledgements

This study was financially supported by the National Natural Science Foundation of China (51579099, 51521006 and 51879105), the Program for Changjiang Scholars and Innovative Research Team in University (IRT-13R17), and the Hunan Provincial Innovation Foundation for Postgraduate (CX2016B134).

## References

- [1] W.P Xiong, Z.T Zeng, X. Li, G.M Zeng, R. Xiao, Z.H Wang, Y.P Zhou, C. Zhang, M. Cheng, L. Hu, C.Y Zhou, L. Qin, R. Xu, Y.P Zhang, Multiwall carbon nanotube/aminomino-functionalized  $\text{Fe}_3\text{O}_4$  composites: remarkable adsorptive removal of antibiotics from aqueous solutions, *Chemosphere* 210 (2018) 1061-1069.
- [2] Y. Yang, Z.T Zeng, C. Zhang, D.P Huang, G.M Zeng, R. Xiao, C. Lai, C.Y Zhou, H. Guo, W.J Xue, M. Cheng, W.J Wang, J.J Wang, Construction of iodine vacancy-rich  $\text{BiOI}/\text{Ag}@\text{AgI}$  Z-scheme heterojunction photocatalysts for visible-light-driven tetracycline degradation: transformation pathways and mechanism insight, *Chem. Eng. J.* 349 (2018) 808-821.
- [3] J. Li, H Zhang, Adsorption-desorption of oxytetracycline on marine sediments: Kinetics and influencing factors, *Chemosphere* 164 (2016) 156-163.
- [4] J.R Pils, D.A Laird, Sorption of tetracycline and chlortetracycline on K- and Ca-saturated soil clays, humic substances, and clay-humic complexes, *Environ. Sci. Technol.* 41 (2007) 1928-1933.
- [5] S.J Ye, G.M Zeng, H.P Wu, C. Zhang, J. Dai, J. Liang, J.F Yu, X.Y Ren, H. Yi, M. Cheng, C. Zhang, Biological technologies for the remediation of co-contaminated soil,

Crit. Rev. Biotechnol. 37 (2017) 1062-1076.

[6] S.J Ye, G.M Zeng, H.P Wu, C. Zhang, J. Liang, J. Dai, Z.F Liu, W.P Xiong, J. Wan, P. Xu, M. Cheng, Co-occurrence and interactions of pollutants, and their impacts on soil remediation—A review, Crit. Rev. Env. Sci. Tec. 47 (2017) , 1528-1553.

[7] H. Wang, H. Yao, P. Sun, D. Li, C.H Huang, Transformation of Tetracycline Antibiotics and Fe(II)/(III) Species Induced by Their Complexation, Environ. Sci. Technol. 50 (2015) 145-153.

[8] L. Qin, G.M Zeng, C. Lai, D.L Huang, P. Xu, C. Zhang, M. Cheng, X.G Liu, S.Y Liu, B.S Li, H. Yi, “Gold Rush” in Modern Science: Fabrication Strategies and Typical Advanced Applications of Gold Nanoparticles in Sensing, Coordin. Chem. Rev. 359 (2018) 1-31.

[9] X.Y Ren, G.M Zeng, L. Tang, J.J Wang, J. Wan, H.P Feng, B. Song, C. Huang, X. Tang, Effect of exogenous carbonaceous material on the bioavailability of organic pollutants and their ecological risks, Soil Biol. Biochem. 116 (2018) 70-81.

[10] X. Jin, S. Qiu, K. Wu, M.Y Ma, F. Wang, C.G Gu, A.Q Zhang, X. Jiang, The effect of Cu<sup>2+</sup> chelation on the direct photolysis of oxytetracycline: A study assisted by spectroscopy analysis and DFT calculation, Environ. Pollut. 214 (2016) 831-839.

[11] Z.Z Huang, P. Xu, G.Q Chen, G.M Zeng, A.W Chen, Z.X Song, K. He, L. Yuan, H. Li, L. Hu, Silver ion-enhanced particle-specific cytotoxicity of silver nanoparticles and effect on the production of extracellular secretions of *Phanerochaete chrysosporium*, Chemosphere 196 (2018) 575-584.

[12] Y.R Wang, Y. Zhu, Y. Hu, G.M Zeng, Y. Zhang, C. Zhang, C.L Feng, How to Construct DNA Hydrogels for Environmental Applications: Advanced Water Treatment and Environmental Analysis, Small 14 (2018), 1-19.

[13] X.Y Gu, Y.Y Tan, F. Tong, C. Gu, Surface complexation modeling of

coadsorption of antibiotic ciprofloxacin and Cu(II) and onto goethite surfaces, Chem. Eng. J. 2015 (269) 113-120.

[14] M. Harja, G. Ciobanu, Studies on adsorption of oxytetracycline from aqueous solutions onto hydroxyapatite, Sci. Total Environ. 628–629 (2018) 36-43.

[15] P. Xu, G.M Zeng, D.L Huang, C.L Feng, S. Hu, M.H Zhao, C. Lai, Z. Wei, C. Huang, G.X Xie, Z.F Liu, Use of iron oxide nanomaterials in wastewater treatment: a review, Sci. Total Environ. 424 (2012) 1-10.

[16] Y. Yang, C. Zhang, C. Lai, G.M Zeng, D.L Huang, M. Cheng, J.J Wang, F. Chen, C.Y Zhou, W.P Xiong, BiOX (X = Cl, Br, I) photocatalytic nanomaterials: Applications for fuels and environmental management, Adv. Colloid. Interfac. 254 (2018) 77-93.

[17] C.Y Zhou, C. Lai, C. Zhang, G.M Zeng, D.L Huang, M. Cheng, L. Hu, W. Xiong, M. Chen, J.J Wang, Y. Yang, L.B Jiang, Semiconductor/boron nitride composites: synthesis, properties, and photocatalytic applications, Appl. Catal. B-Environ. 238 (2018) 6-18.

[18] H. Wang, Y.H Dong, X.Y. Yang, G. Toor, X.M zhang, Changes in heavy metal contents in animal feeds and manures in an intensive animal production region of China, J. Environ. Sci. 25 (2013), 2435-2442.

[19] Z.Z Huang, P. Xu, G.Q Chen, G.M Zeng, A.W Chen, Z.X Song, K. He, L. Yuan, H. Li, L.Hu, Silver ion-enhanced particle-specific cytotoxicity of silver nanoparticles and effect on the production of extracellular secretions of *Phanerochaete chrysosporium*, Chemosphere 196 (2018) 575-584.

[20] Z.Z Huang, Z.T Zeng, A.W Chen, G.M Zeng, R. Xiao, P. Xu, K. He, Z.X Song, L.Hu, M. Peng, T.T Huang, G.Q Chen, Differential behaviors of silver nanoparticles and silver ions towards cysteine: Bioremediation and toxicity to *Phanerochaete*

*chrysosporium*, Chemosphere 203 (2018) 199-208.

[21] L.H Zhang, J.C Zhang, G.M Zeng, H.R Dong, Y.N Chen, C. Huang, Y. Zhu, R. Xu, Y.J Cheng, K.J Hou, W.C Cao, W. Fang, Multivariate relationships between microbial communities and environmental variables during co-composting of sewage sludge and agricultural waste in the presence of PVP-AgNPs, Bioresource Technol. 261 (2018) 10-18.

[22] X. Tang, G.M Zeng, C.Z Fan, M. Zhou, L. Tang, J.J Zhu, J. Wan, D.L Huang, M. Chen, P. Xu, C. Zhang, W.P Xiong, Chromosomal expression of CadR on *Pseudomonas aeruginosa* for the removal of Cd(II) from aqueous solutions, Sci. Total Environ. 636 (2018) 1355–1361.

[23] B. Carlotti, A. Cesaretti, F. Elisei, Complexes of tetracyclines with divalent metal cations investigated by stationary and femtosecond-pumped techniques, Phys. Chem. Chem. Phys. 14 (2011), 823-834.

[24] L. Chen, J.H Li, L.X Chen, Colorimetric Detection of Mercury Species Based on Functionalized Gold Nanoparticles, ACS Appl. Mater. Inter. 6 (2014) 15897-15904.

[25] Y.P Zhao, Y.Y Tan, X. Guo, X.Y Gu, X.R Wang, Y. Zhang, Interactions of tetracycline with Cd (II), Cu (II) and Pb (II) and their cosorption behavior in soils, Environ. Pollut. 180 (2013) 206-213.

[26] H. Yi, D.L Huang, L. Qin, G.M Zeng, C. Lai, M. Cheng, S.J Ye, B. Song, X.Y Ren, X.Y Guo, Selective Prepared Carbon Nanomaterials for Advanced Photocatalytic Application in Environmental Pollutant Treatment and Hydrogen Production, Appl. Catal. B-Environ. 239 (2018) 408-424.

[27] K. He, Z.T Zeng, A.W Chen, G.M Zeng, R. Xiao, P. Xu, Z.Z Huang, J.B Shi, L. Hu, G.Q Chen, Advancement of Ag-graphene based nanocomposites: An overview on synthesis and its applications, Small 14 (2018) 1-13.

- [28] Y. Zhang, X.Y Cai, X.M Lang, X.L Qiao, X.H Li, J.W Chen, Insights into aquatic toxicities of the antibiotics oxytetracycline and ciprofloxacin in the presence of metal: complexation versus mixture, *Environ. Pollut.* 166 (2012) 48-56.
- [29] M.Y Jia, F. Wang, X. Jin, Y. Song, Y.R Bian, L.A Boughner, X.L Yang, C.G Gu, X. Jiang, Q.G Zhao, Metal ion–oxytetracycline interactions on maize straw biochar pyrolyzed at different temperatures, *Chem. Eng. J.* 304 (2016) 934-940.
- [30] A.W Chen, C. Shang, J.H Shao, Y.Q Lin, S. Luo, J.C Zhang, H.L Huang, M. Lei, Q.R Zeng, Carbon disulfide-modified magnetic ion-imprinted chitosan-Fe(III): A novel adsorbent for simultaneous removal of tetracycline and cadmium, *Carbohydr. Polym.* 155 (2017) 19-27.
- [31] Z.Y Zhang, H.J Liu, L.Y Wu, H.C Lan, J.H Qu, Preparation of amino-Fe(III) functionalized mesoporous silica for synergistic adsorption of tetracycline and copper, *Chemosphere* 138 (2015) 625-632.
- [32] G.G Wu, J.P Ma, S. Li, J. Guan, F. Jiang, L.Y Wang, J.H Li, X.Y Wang, L.X Chen, Magnetic copper-based metal-organic framework as an effective and recyclable adsorbent for removal of two fluoroquinolone antibiotics from aqueous solutions, *J. Colloid Inter. Sci.* 528 (2018) 360-371.
- [33] M.K Uddin, A review on the adsorption of heavy metals by clay minerals, with special focus on the past decade, *Chem. Eng. J.* 308 (2017) 438-462.
- [34] M.F Li, Y.G Liu, S.L Liu, D. Shu, G.M Zeng, X.J Hu, X.F Tan, L.H Jiang, Z.L Yan, X.X Cai, Cu(II)-influenced adsorption of ciprofloxacin from aqueous solutions by magnetic graphene oxide/nitrilotriacetic acid nanocomposite: Competition and enhancement mechanisms, *Chem. Eng. J.* 319 (2017) 219-228.
- [35] X.Y Gu, Y.Y Tan, F. Tong, C. Gu, Surface complexation modeling of coadsorption of antibiotic ciprofloxacin and Cu(II) and onto goethite surfaces, *Chem.*

Eng. J. 269 (2015) 113-120.

[36] Y.J Wang, D.A Jia, R.J Sun, H.W Zhu, D.M Zhou, Adsorption and cosorption of tetracycline and copper(II) on montmorillonite as affected by solution pH, Environ. Sci. Technol. 42 (2008) 3254-3259.

[37] M. Othmani, A. Aissa, C.G Bac, F. Rachdi, M. Debbabi, Surface modification of calcium hydroxyapatite by grafting of etidronic acid, Appl. Surf. Sci. 274 (2013) 151-157.

[38] D.J Wang, L.Y Chu, M. Paradelo, W.J Peijnenburg, Y.J Wang, D.M zhou, Transport behavior of humic acid-modified nano-hydroxyapatite in saturated packed column: Effects of Cu, ionic strength, and ionic composition, J. Colloid Interf. Sci. 360 (2011) 398-407.

[39] S. Cazalbou, G. Bertrand, C. Drouet, Tetracycline Loaded Biomimetic Apatite: An Adsorption Study, J. Phys. Chem. B 109 (2005) 3014-3024.

[40] Y.M Li, S.G Wang, Y. Zhang, R.M Han, W. Wei, Enhanced tetracycline adsorption onto hydroxyapatite by Fe(II) incorporation, J. Mol. Liq. 2017 (247) 171-181.

[41] R.A Figueroa, A.A Mackay, Sorption of oxytetracycline to iron oxides and iron oxide-rich soils, Environ. Sci. Technol. 39 (2005), 6664-6671.

[42] Z.Z Huang, G.Q Chen, G.M Zeng, Z. Guo, K. He, L. Hu, J. Wu, L.H Zhang, Y. Zhu, Z.X Song, Toxicity mechanisms and synergies of silver nanoparticles in 2,4-dichlorophenol degradation by *Phanerochaete chrysosporium*, J. Hazard. Mater. 321 (2016) 37-46.

[43] L. Hu, J. Wan, G.M Zeng, A.W Chen, G.Q Chen, Z.Z Huang, K. He, M. Cheng, C.Y Zhou, W.P Xiong, C. Lai, P. Xu, Comprehensive evaluation of the cytotoxicity of CdSe/ZnS quantum dots in *Phanerochaete chrysosporium* by cellular uptake and

oxidative stress, *Environ. Sci. Nano* 4 (2017) 2018-2029.

[44] Z.Z Huang, G.Q Chen, G.M Zeng, A.W Chen, Y.N Zuo, Q. Tian, Z.X Song, Q.Y Niu, Polyvinyl alcohol-immobilized *Phanerochaete chrysosporium*, and its application in the bioremediation of composite-polluted wastewater, *J. Hazard. Mater.* 289 (2015).

[45] N. Tang, C.G Niu, X.T Li, C. Liang, H. Guo, L.S Lin, C.W Zheng, G.M Zeng, Efficient removal of  $\text{Cd}^{2+}$  and  $\text{Pb}^{2+}$  from aqueous solution with amino- and thiol-functionalized activated carbon: Isotherm and kinetics modeling, *Sci. Total Environ.* 635 (2018) 1331-1344.

[46] P.C Lombardo, A.L Poli, L.F Castro, J.R Perussi, C.C Schmit, Photochemical Deposition of Silver Nanoparticles on Clays and Exploring their Antibacterial Activity, *Acs Appl. Mater. Inter.* 8 (2016) 21640-21647.

[47] L. El Hammari, H. Merroun H, T. Coradin, S. Cassaignon, A. Laghizil, A. Saoiabi, Mesoporous hydroxyapatites prepared in ethanol–water media: Structure and surface properties, *Mater. Chem. Phys.* 104 (2007) 448-453.

[48] Z.Z Zhang, M.Y Li, W. Chen, S.Z Zhu, N.N Liu, L.Y Zhu, Immobilization of lead and cadmium from aqueous solution and contaminated sediment using nano-hydroxyapatite, *Environ. Pollut.* 158 (2010) 514-519.

[49] H. Nishida, M. Kimata, T. Ogata, T. Kawei, Malodors adsorption behavior of metal cation incorporated hydroxyapatite, *J. Environ. Chem. Eng.* 5 (2017) 2815-2819.

[50] M.Y Jia, F. Wang F, Y.R Bian, X. Jin, Y. Song, F.O kengara, R.K Xu, X. Jiang, Effects of pH and metal ions on oxytetracycline sorption to maize-straw-derived biochar, *Bioresour. Technol.* 136 (2013) 87-93.

[51] W. Zhang, F.H Wang, P.L Wang, L. Lin, Y. Zhao, P. Zou, M.J Zhao, H. Chen, Y. Liu, Y.S Zhang, Facile synthesis of hydroxyapatite/yeast biomass composites and

their adsorption behaviors for lead (II), J. Colloid Inter. Sci. 477 (2016) 181-190.

[52] L. Chen , K.S Zhang, J.Y He, W.H Xu, X.J Huang, J.H Liu, Enhanced fluoride removal from water by sulfate-doped hydroxyapatite hierarchical hollow microspheres, Chem. Eng. J. 285 (2016) 616-624.

[53] X.Q Cai, J.H Li, Z. Zhang, F.F Yang, R.C Dong, L.X Chen, Novel Pb<sup>2+</sup> ion imprinted polymers based on ionic interaction via synergy of dual functional monomers for selective solid-phase extraction of Pb<sup>2+</sup> in water samples, Acs Appl. Mater. Inter. 6 (2014) 305-313.

[54] H. Wang, H. Yao, P. Sun, C.H Huang, Oxidation of tetracycline antibiotics induced by Fe(III) ions without light irradiation, Chemosphere 119 (2015) 1255-1261.

[ 55 ] M. Jezowska-bojczuk, L. Lambs, H. Kozłowski, G. Berthon, Metal ion-tetracycline interactions in biological fluids. 10. Structural investigations on copper(II) complexes of tetracycline, oxytetracycline, chlortetracycline, 4-(dedimethylamino)tetracycline, and 6-desoxy-6-demethyltetracycline and discussion of their binding modes, Inorg. Chem. 32 (1993):428-437.

[56] M.A Ghandou, H.A Azab, A. Hassan, A.M Ali, Potentiometric studies on the complexes of tetracycline (TC) and oxytetracycline (OTC) with some metal ions, Monatsh. Chem. 123 (1992) 51-58.

[57] Z. Yang, S.Y Jia, T.T Zhang, N. Zhuo, Y.Y Dong, W.B Yang, Y.P Yang, How heavy metals impact on flocculation of combined pollution of heavy metals–antibiotics: A comparative study, Sep. Purif. Technol. 149 (2015) 398-406.

[ 58 ] M. Novák-Páľi, E.H Mesbah, G. Pethő, Equilibrium studies on tetracycline-metal ion systems, J. Pharmaceut. Biomed. 14 (1996) 1025-1029.

[59] J. M. Wessels, W.E Ford, W. Szymczak, S. Schneider, The Complexation of Tetracycline and Anhydrotetracycline with Mg<sup>2+</sup> and Ca<sup>2+</sup>: A Spectroscopic Study, J.

Phys. Chem. B 102 (1998) 9323-9331.

[60] Y. Xu, F.W Schwartz, S.Y Traina, Sorption of  $\text{Zn}^{2+}$  and  $\text{Cd}^{2+}$  on Hydroxyapatite Surfaces, Environ. Sci. Technol. 28 (1994) 1472-1480.

[61] E. Mavropoulos, A.M Rossi, A.M Costa, C.A Perez, J.C Moreira, M. Saldanha, Studies on the Mechanisms of Lead Immobilization by Hydroxyapatite, Environ. Sci. Technol. 36 (2002) 1625-1629.

[62] P.L Nostro, V. Mazzini, B.W Ninham, M. Ambrosi, L.G Dei, P. Baglioni, Specific anion effect on the kinetics of iodination of acetone, Chemphyschem, 17 (2016) 2567-2571.

[63] P.S Pinto, T.P Medeiros, J.D Ardisson, R.M Lago, Role of  $[\text{FeO}_x(\text{OH})_y]$  surface sites on the adsorption of  $\beta$ -lactamic antibiotics on  $\text{Al}_2\text{O}_3$  supported Fe oxide, J. Hazard. Mater. 317 (2016) 327-334.

[64] Z. Zhang, H. Liu, L. Wu, H. Yan, J. Qu, Preparation of amino-Fe(III) functionalized mesoporous silica for synergistic adsorption of tetracycline and copper, Chemosphere 138 (2015) 625-632.

[65] J. Kang, H. Liu, Y.M. Zheng, J.P Chen, Systematic study of synergistic and antagonistic effects on adsorption of tetracycline and copper onto a chitosan, J. Colloid Inter. Sci. 344 (2010) 117-125.

[66] C. Chen, J.J Dynes, J. Wang, D.L Sparks, Properties of Fe-organic matter associations via coprecipitation versus adsorption, Environ. Sci. Technol. 48 (2014), 48 13751-13759.

[67] R. Yang, Z.W Li, B. Huang, N.L Luo, M. Huang, J.J Wen, Q. Zhang, X.Q Zhai, G.M Zeng, Effects of Fe(III)-fulvic acid on Cu removal via adsorption versus coprecipitation, Chemosphere 197 (2018) 291-298.

[68] B.Y Huang, Y.G Liu, B. Li, S.B Liu, G.M Zeng, Z.W Zeng, X.H Wang, Q.M

Ning, B.H Zheng, C.P Yang, Effect of Cu(II) ions on the enhancement of tetracycline adsorption by  $\text{Fe}_3\text{O}_4@\text{SiO}_2$ -Chitosan/graphene oxide nanocomposite, Carbohydr. Polym. 157 (2017) 576-585.

Accepted MS